

Fragment-based design for the development of N-domain-selective angiotensin-1-converting enzyme inhibitors

Ross G. DOUGLAS*¹, Rajni K. SHARMA†¹, Geoffrey MASUYER‡, Lizelle LUBBE*, Ismael ZAMORA§, K. Ravi ACHARYA‡, Kelly CHIBALE† and Edward D. STURROCK*

*Institute of Infectious Disease and Molecular Medicine, and Division of Medical Biochemistry, University of Cape Town, Observatory, Cape Town 7935, South Africa

†Department of Chemistry and Institute of Infectious Disease and Molecular Medicine, University of Cape Town, Rondebosch, Cape Town 7701, South Africa

‡Department of Biology and Biochemistry, University of Bath, Claverton Down, Bath BA2 7AY, U.K.

§Lead Molecular Design, Sant Cugat del Vallès and Pompeu Fabra University, Barcelona, Spain

Abstract

ACE (angiotensin-1-converting enzyme) is a zinc metallopeptidase that plays a prominent role in blood pressure regulation and electrolyte homeostasis. ACE consists of two homologous domains that despite similarities of sequence and topology display differences in substrate processing and inhibitor binding. The design of inhibitors that selectively inhibit the N-domain (N-selective) could be useful in treating conditions of tissue injury and fibrosis due to build-up of N-domain-specific substrate Ac-SDKP (*N*-acetyl-Ser-Asp-Lys-Pro). Using a receptor-based SHOP (scaffold hopping) approach with N-selective inhibitor RXP407, a shortlist of scaffolds that consisted of modified RXP407 backbones with novel chemotypes was generated. These scaffolds were selected on the basis of enhanced predicted interaction energies with N-domain residues that differed from their C-domain counterparts. One scaffold was synthesized and inhibitory binding tested using a fluorogenic ACE assay. A molecule incorporating a tetrazole moiety in the P₂ position (compound **33RE**) displayed potent inhibition ($K_i = 11.21 \pm 0.74$ nM) and was 927-fold more selective for the N-domain than the C-domain. A crystal structure of compound **33RE** in complex with the N-domain revealed its mode of binding through aromatic stacking with His³⁸⁸ and a direct hydrogen bond with the hydroxy group of the N-domain specific Tyr³⁶⁹. This work further elucidates the molecular basis for N-domain-selective inhibition and assists in the design of novel N-selective ACE inhibitors that could be employed in treatment of fibrosis disorders.

Key words: angiotensin-1-converting enzyme (ACE), crystal structure, *in silico* screening, inhibitor design, kinetics, RXP407

INTRODUCTION

ACE (angiotensin-1-converting enzyme; EC 3.4.15.1) is a zinc dipeptidyl carboxypeptidase that plays a critical role in blood pressure regulation and electrolyte homeostasis [1,2]. ACE consists of two catalytic domains (designated N- and C-domains) that, despite high-sequence identity and structural topology, display differences in substrate processing and inhibitor binding [3–6]. Studies involving the generation of mice containing one domain catalytically inactivated have provided important insight into the differing roles of the two domains. *In vivo* both domains clear the vasodilator peptide bradykinin with approximately equal efficiencies [7–9], the C-domain appears to be the prominent

site for the production of vasoactive peptide angiotensin II, whereas the N-domain is the primary site for the clearance of tetrapeptide Ac-SDKP (*N*-acetyl-Ser-Asp-Lys-Pro) [8–10]. Ac-SDKP was first discovered owing to its ability to halt differentiation of the haematopoietic system [11,12]. More recent work has emphasized a potent anti-inflammatory and anti-fibrotic role in heart, liver, kidney and lung tissues [13–25]. Furthermore, Ac-SDKP levels have been shown to increase in patients acutely treated with ACE inhibitors [26] and suggests a possible therapeutic strategy for treating diseases involving fibrosis.

There are a number of ACE inhibitors that have been approved for clinical use [27]. These inhibitors inhibit both domains with similar affinity in the low nanomolar range [28]. While this

Abbreviations: ACE, angiotensin-1-converting enzyme; Ac-SDKP, *N*-acetyl-Ser-Asp-Lys-Pro; N-selective, N-domain selective; SHOP, scaffold hopping.

¹These authors contributed equally to this work.

Correspondence: Professor Edward D. Sturrock (email edward.sturrock@uct.ac.za), Professor Kelly Chibale (email kelly.chibale@uct.ac.za) or Professor K. Ravi Acharya (email K.R.Acharya@bath.ac.uk).

Table 1 A summary of relevant ACE substrates and inhibitors

Domain contribution	Substrate	Biological action of substrate	Biological action of product after ACE hydrolysis	Inhibitor(s) targeting the indicated domain
Both domains approximately equally	Bradykinin	Vasodilation	Inactive	Captopril, lisinopril, enalaprilat, ramiprilat and others [27]
C-domain specific	Angiotensin(1–7)	Vasodilation	Inactive	
C-domain specific	Angiotensin I	Inactive	Vasoconstriction, hypertrophy and fibrosis	RXPA380 [50], lisinopril-Trp [51], and inhibitors kAW and kAF [52]
N-domain specific	N-Acetyl-SDKP	Anti-fibrosis	Inactive	RXP407 [32]

allows for effective reduction in blood pressure, adverse drug effects result, possibly due to excessive bradykinin accumulation by dual domain blockade [29–31]. Thus selective inhibition of one ACE domain could allow for effective treatment with reduced adverse event incidence. More specifically, N-selective (N-domain-selective) inhibition could allow for the treatment of tissue injury and fibrosis diseases without affecting blood pressure and with reduced side effect profiles (Table 1).

RXP407 is a phosphinic peptidomimetic ACE inhibitor that displays approximately three orders of magnitude N-selectivity [32]. Detailed structure–activity studies revealed the importance of the *N*-acetyl group, P₂ aspartate residue and C-terminal amide as contributors to the observed N-selectivity [32]. Using this information, we previously designed and synthesized ketomethylene inhibitors that incorporated the above functionalities either alone or in combination and showed that the incorporation of the P₂ aspartate residue and *N*-protecting group resulted in a 1000-fold shift towards N-selectivity [33].

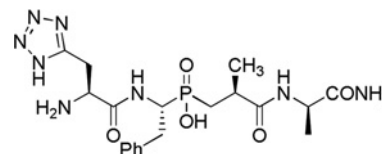
Elucidation of the ACE domain structures has allowed for the understanding of active site architecture and the relative positioning of amino acids that differ between the two domains [5,6]. Furthermore, the determination of the RXP407 co-crystallized with the N-domain shows that, of all the unique amino acids present, only prominent contacts with the unique residues Tyr³⁶⁹ and Arg³⁸¹ (by the P₂ aspartate residue) were exploited by the inhibitor [34]. This observation is consistent with a mutagenic study [35]. Structural information such as that above provides detailed binding modes of ligands in their respective active sites and can be utilized to generate scaffolds with similar or improved binding affinities with novel functionalities.

It was the purpose of the present study to exploit unique N-domain residue interactions with novel chemotypes using a receptor-based SHOP (scaffold hopping) GRID-based molecular modelling approach [36,37]. Such an approach has enabled the identification of potentially useful fragments that are not limited to natural amino acid residues. Furthermore, this approach has allowed for the production of a novel ACE inhibitor that is a potent inhibitor and displays approximately 1000-fold N-selectivity.

MATERIALS AND METHODS

Modelling methodology and synthesis

SHOP methodology was employed to screen for commercially available building blocks that would possess similar or improved

**Figure 1** Structure of compound 33RE

active site interaction properties (the procedure is outlined in the Supplementary Materials and methods section at <http://www.clinsci.org/cs/126/cs1260305add.htm>). Four amino acids differing in chemical nature from their C-domain counterparts were selected. Residues Tyr³⁶⁹ and Arg³⁸¹ are located in the S₂ subsite and have been shown by both mutagenesis and structural studies to be important for selective RXP407 binding [34,35]. These amino acids are replaced by Phe³⁹¹ and Glu⁴⁰³, respectively, in the C-domain (all C-domain residues are given as tACE numbering). Thr⁴⁹⁶ is located on the border of the S₂ and S₁ subsites [6]. Owing to its proximity to the RXP407 Phe and the lack of hydrogen bonding potential of the corresponding C-domain residue (Val⁵¹⁸), it was selected as a side-chain for further selective binding exploitation by hydrogen bonding. Thr³⁵⁸ is located in the S₂' subsite and differs from the corresponding C-domain residue Val³⁸⁰ [6]. As with Thr⁴⁹⁶, identification of functional groups that allows for specific interaction with the threonine side chain by hydrogen bonding could assist in generating N-selective inhibitors. Novel inhibitor structures that met the criteria were selected for further study. Final compound 33RE (Figure 1) was synthesized using established synthetic approaches and purified to homogeneity (Supplementary Materials and methods section and Scheme S1 at <http://www.clinsci.org/cs/126/cs1260305add.htm>).

Inhibition characterization

Parent molecule RXP407 and compound 33RE were dissolved in sterile distilled water to yield stock solutions of 10 mM and subsequently serially diluted in assay buffer (50 mM Hepes, pH 6.8, 200 mM NaCl and 10 μM ZnSO₄). Assays were performed on wild-type N-domain, C-domain and N-domain S₂ mutants Y369F, R381E and YR/FE as described previously [32,35]. Briefly, 40 nM enzyme was incubated with an equi-volume amount of an appropriate concentration range of phosphinic inhibitor at ambient temperature for 5 min. Enzyme-inhibitor solutions were then divided into aliquotes in triplicate 20 μl volumes followed by the addition of 280 μl of fluorogenic substrate (Abz)-FRK(Dnp)P-OH (in assay buffer) to yield a final

substrate concentration of 4 or 8 μM . Residual enzyme activity was monitored continuously at $\lambda_{\text{ex}} = 320 \text{ nm}$ and $\lambda_{\text{em}} = 420 \text{ nm}$ using a fluorescence spectrophotometer (Cary Eclipse, Varian). Initial change of fluorescence over time was converted into arbitrary rate units and inhibitor-binding affinities determined using the Dixon method [38].

Protein purification and X-ray crystallography

N-domain ACE was expressed and purified to homogeneity from CHO (Chinese-hamster ovary) cells [39]. The crystals of the N-domain ACE complex with 33RE were grown at 16°C by the hanging drop vapour diffusion method. N-domain ACE (5 mg/ml in 50 mM Hepes, pH 7.5) was pre-incubated with 33RE (3.3 mM) at room temperature (20°C) for 2 h before crystallization. Pre-incubated sample (1 μl) was mixed with the reservoir solution consisting of 30% PEG550 MME/PEG20000, 100 mM Tris/Bicine, pH 8.5, and 0.06 M divalent cations (Molecular Dimensions), and suspended above the well. Crystals appeared within 3 days.

X-ray diffraction data for the N-domain ACE–33RE complex were collected on the PX station IO4-1 at Diamond Light Source (Didcot). A total of 720 images were collected using a Quantum-4 CCD (charge-coupled-device) detector (ADSC Systems). No cryoprotectant was used and the crystal was kept at constant temperature (100 K) under the liquid nitrogen jet during data collection. Raw data images were indexed and scaled with XDS [40] and the CCP4 program SCALA [41]. Initial phasing for structure solution was obtained using the molecular replacement routines of the program PHASER [42]. The atomic co-ordinates of N-domain ACE [34] (PDB code 3NXQ) were used as a search model. The resultant model was refined using REFMAC5 [43] and adjustment of the model was carried out using COOT [44]. Water molecules were added at positions where $F_o - F_c$ electron density peaks exceeded 3σ and potential H-bonds could be made. On the basis of the electron density interpretation, the inhibitor and glycosylated carbohydrate moieties were added in the complex structure and further refinement was carried out. The co-ordinate and parameter files for 33RE were generated using SKETCHER [41] and validated through the PRODRG server [45]. Validation of the protein structure was conducted with the aid of MOLPROBITY [46]. Figures were drawn with PyMOL (DeLano Scientific). Hydrogen bonds were verified with the program HBPLUS [47]. The detailed refinement statistics for the complex structure are given in Table 2.

RESULTS

The SHOP modelling procedure yielded a list of fragments. Compounds containing novel functionalities were redocked into the N-domain active site. Those which had prominent interactions with identified amino acid side-chains were scored on the basis of interaction energies. This approach resulted in a short list of compounds that had interactions that were equal or improved compared to parent molecule RXP407 (Table 3). Compound 33RE (Figure 1) was selected for synthesis and inhibition analysis given

Table 2 Crystallographic statistics of N-ACE–33RE complex
Values in parentheses are for last resolution shell.

Parameter	
Resolution (Å)	2.2
Space group	P1
Cell	a = 73.1, b = 77.3, c = 82.9 $\alpha = 88.4, \beta = 64.3, \gamma = 75.3$
Number of molecules in ASU	2
Redundancy	3.9 (3.9)
Total/unique reflections	281360/73018
Completeness (%)	91.4 (88.7)
R_{sym}^*	12.5 (84.6)
$I/\sigma(I)$	10.5 (2.6)
R_{cryst}^\dagger	18.8
R_{free}^\ddagger	21.9
R_{msd} bond (Å)	0.008
R_{msd} angle ($^\circ$)	1.18
B-factor analysis	
Protein all atom (chain A/B)	26.0/30.3
Protein main chain (chain A/B)	25.5/29.8
Protein side atoms (chain A/B)	26.4/30.8
Zinc ion (chain A/B)	17.6/14.2
Chloride ion (chain A/B)	17.4/22.7
Inhibitor (chain A/B)	21.3/18.2
Sugars (chain A/B)	47.6/59.1
Solvent	25.8
PDB code	4BXK

* $R_{\text{sym}} = \sum_h \sum_i |I_i(h) - \langle I(h) \rangle| / \sum_h \sum_i I_i(h)$, where I_i is the i th measurement and $\langle I(h) \rangle$ is the weighted mean of all the measurements of $I(h)$
† $R_{\text{cryst}} = \sum_h |F_o - F_c| / \sum_h F_o$, where F_o and F_c are observed and calculated structure factor amplitudes of reflection h respectively
‡ R_{free} is equal to R_{cryst} for a randomly selected 5% subset of reflections.

the prominence of the P₂ position in conferring N-selectivity and the presence of a non-carboxylate moiety in this position (Figure 2). This fragment can replace the original one from RXP407 with similar interactions (Figure 3).

A classical and relatively straightforward 6-step synthetic approach resulted in the production of compound 33RE in modest yields. Furthermore, this process possesses the possibility of scalability to larger amounts for further pharmacokinetic and preclinical testing.

Assessment of inhibitor potential was carried out using a continuous fluorogenic assay (Abz)-FRK(Dnp)P assay. Compound 33RE displayed low nanomolar inhibition of the N-domain ($K_i = 11.21 \pm 0.74 \text{ nM}$) in a similar range to parent molecule RXP407 ($K_i = 21.03 \pm 0.27 \text{ nM}$). Characterization of the C-domain showed micromolar inhibition with compound 33RE ($K_i = 10\,395 \pm 593 \text{ nM}$) as well as RXP407 ($K_i = 60\,826 \pm 9\,175 \text{ nM}$), thus both compounds displayed three orders of magnitude N-selectivity (Table 4 and Figure 4). The active site mutants Y369F and R381E showed a marked decreased affinity for compound 33RE ($K_i = 404.4 \pm 17.25 \text{ nM}$ and $K_i = 86.97 \pm 6.29 \text{ nM}$, respectively) compared with wild-type N-domain. Upon substitution of both these residues in the double mutant YR/FE an additive effect was observed

Table 3 Summary of results obtained from SHOP methodology

R^2 is given relative to the crystal structure RXP407 ligand backbone. Interaction energies of S_2 , S_1 and S_2' amino acids of modified ligands compared with RXP407 are given in red, orange and purple respectively.

Name	Structure	R^2 (Å)	Residue interaction energies (kcal/mol)
RXP407		1	
33RE		0.85	
2B-004		0.73	
1X-0802		0.65	
HC-6004		0.98	
CA-4124		0.95	
AF-399		0.72	
BTB-08399		0.66	
JCC-0014		0.59	

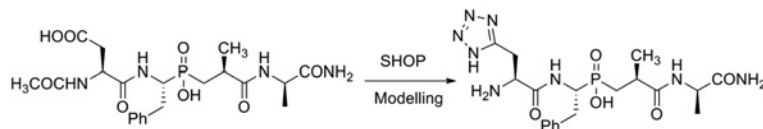


Figure 2 Fragment suggested to have complementary interactions with the protein in the same region as the one originally selected from 3NXQ [34]

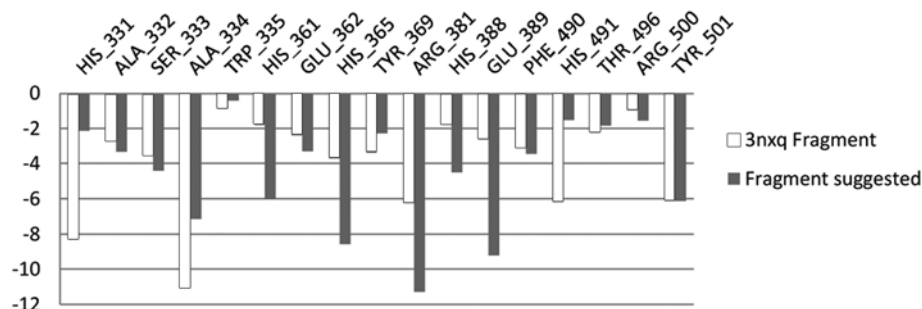


Figure 3 Interaction energies for all of the amino acids in the binding site for both RXP407[34] and compound 33RE

($K_i = 2794 \pm 156$ nM), which led to a drastic decrease in 33RE selectivity (only ~4-fold N-selectivity compared with 927-fold with wild-type). Given the importance of these two residues in conferring selectivity for both 33RE and parent molecule RXP407, the kinetic results suggest that the actual interaction energies for the two inhibitors with these residues is critical [35].

The co-crystal structure of N-domain ACE was solved at 2.2 Å in complex with compound 33RE (Figure 5). The crystals obtained were similar to those described by Anthony et al. [34] and diffracted in space group $P1$ with 2 molecules per asymmetric unit (Table 2). In both the molecules, clear electron density was visible for the entire ligand (Figure 6A), and allowed for a precise description of the molecular interactions responsible for inhibition. The backbone of 33RE binds to N-domain ACE in a similar way to RXP407 with the central phosphate group coordinating with the catalytic zinc ion (Figure 6B and Table 5) and residues Tyr⁵⁰¹ and His³⁶⁵. The mode of binding at the P_2' site is identical for the two inhibitors through hydrogen bonds with residues Lys⁴⁸⁹ and Tyr⁴⁹⁸, and also at the P_1' site where they can both make contact with His³³¹ and His⁴⁹¹. The P_1 site is stabilized within the catalytic channel through hydrophobic interactions, particularly with Phe⁴⁹⁰, Ser³³³ and Thr⁴⁹⁶, and with a water-mediated interaction with Tyr⁵⁰¹ and Arg⁵⁰⁰.

The differences between compounds RXP407 and 33RE reside at position P_2 . Although the backbone remains well

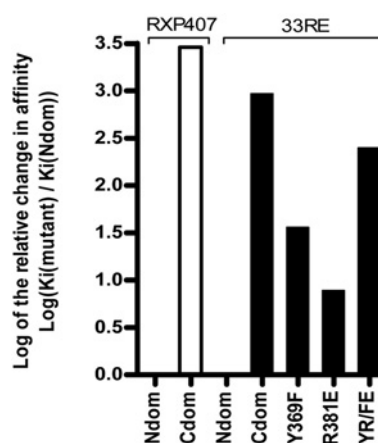


Figure 4 Logarithmic scale comparison of the relative 33RE-binding affinity of N-domain mutants with that of the wild-type domains (black bars)

Relative binding affinity of wild-type domains for RXP407 is shown as white bars. Positive values represent decreased affinity relative to the unmutated N-domain, thus towards more C-domain-like K_i .

anchored in S_2 by a hydrogen bond with Ala³³⁴, modification of aspartate at P_2 resulted in the loss of a potential water-mediated interaction with its C-terminal end and the amido group of Asp³³⁶.

Table 4 Inhibitor-binding constants (K_i) determined for wild-type proteins and S_2 mutants

Values are means \pm S.E.M. C/N, C-terminal/N-terminal.

Construct	RXP407 K_i (nM)	Fold selectivity K_i (C/N)	33RE K_i (nM)	Fold selectivity K_i (C/N)
N-domain	21.03 \pm 0.27	2896	11.21 \pm 0.74	927
C-domain	60 826 \pm 9 175		10 395 \pm 593	
Y369F	n.d.*	n.d.*	404.4 \pm 17.3	26
R381E	n.d.*	n.d.*	86.97 \pm 6.29	120
YR/FE	n.d.*	n.d.*	2794 \pm 156	4

*Not determined in the study [35].

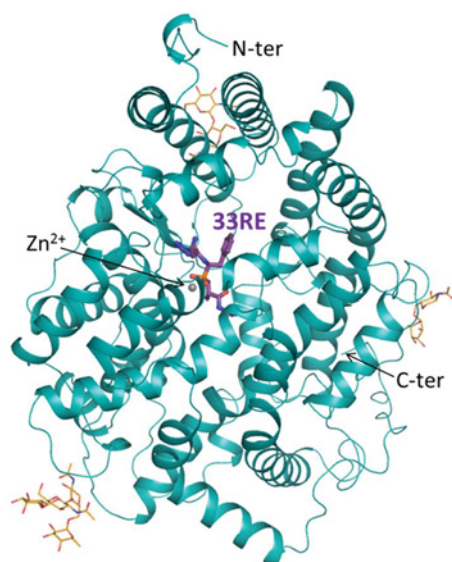


Figure 5 Crystal structure of N-domain ACE in complex with compound 33RE

ACE is shown in cartoon representation (cyan) with catalytic zinc ion as a grey sphere, and glycosyl chains as orange sticks. Compound **RE33** is represented in purple.

In addition, modification of the acidic side-chain caused the loss of the salt bridge with Arg³⁸¹, which resulted in the reorientation of its long side chain away from the active site (Figure 7). However, inclusion of the tetrazole moiety allowed an alternative mode of binding of **33RE** through aromatic stacking with His³⁸⁸ and direct hydrogen bond with the hydroxy group of N-domain-specific Tyr³⁶⁹. Furthermore, a network of water molecules was clearly observed and stabilizes the compound in S₂; particularly, water-mediated interactions were observed with Tyr³⁶⁹ on the one

Table 5 Potential hydrogen bonds of **33RE** binding to N-ACE

Residue	Atom	33RE	Distance (Å)
P2'			
Tyr ⁴⁹⁸	OH	O	2.5
Lys ⁴⁸⁹	NZ	O	2.8
Water 1	O	NAC	2.7
P1'			
His ³³¹	NE2	OAF	2.9
His ⁴⁹¹	NE2	OAF	3.0
Phosphate			
Tyr ⁵⁰¹	OH	OAH	2.7
	Zn ²⁺	OAH	2.0
	Zn ²⁺	OAI	2.5
His ³⁶⁵	NE2	OAI	3.1
P1			
Water 2	O	NAV	3.0
P2			
Ala ³³⁴	N	OAG	2.8
Tyr ³⁶⁹	OH	NAS	2.7
Water 3	O	NAT	3.1
Water 4	O	NAR	3.1

side and potential interactions with Glu³⁸⁹, Arg⁵⁰⁰ and Pro³⁸⁵ on the other side (Figure 6A).

DISCUSSION

ACE inhibitors remain an effective therapeutic strategy in the treatment of cardiovascular disease. With the prominent anti-fibrotic and anti-inflammatory effects of Ac-SDKP evident,

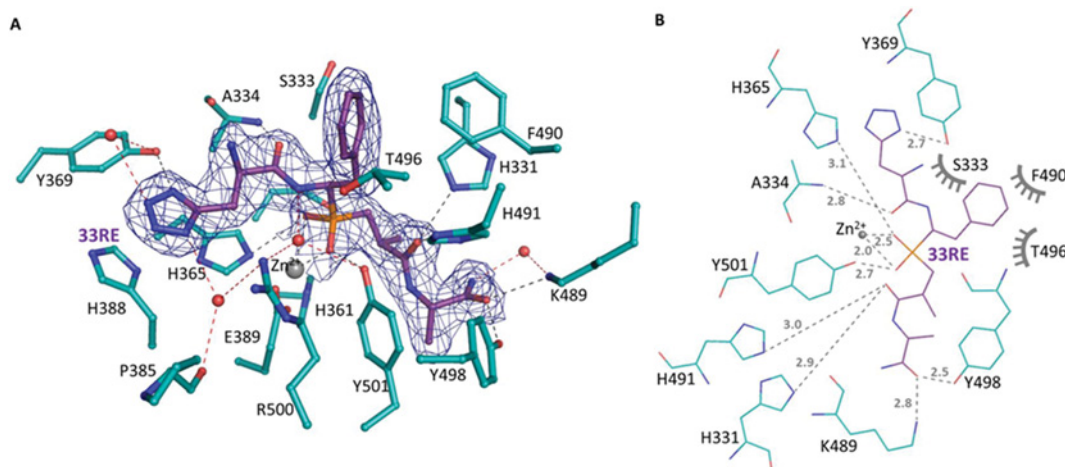


Figure 6 Binding of compound **33RE** to N-domain ACE

(A) Residues of N-domain ACE (cyan) interacting with **33RE** (purple) are shown as sticks. Potential hydrogen bonds and water-mediated interactions are shown as black and red dash lines respectively. Electron density (blue) corresponds to omit map for **33RE** at 1 σ . Water and zinc ions are represented as red and grey spheres respectively. (B) Schematic diagram of potential hydrogen bonds (dashed lines, distances in Å; where 1 Å = 0.1 nm) and hydrophobic interactions (grey symbols) between N-domain ACE (cyan) and **33RE** (purple) obtained from LIGPLOT [49].

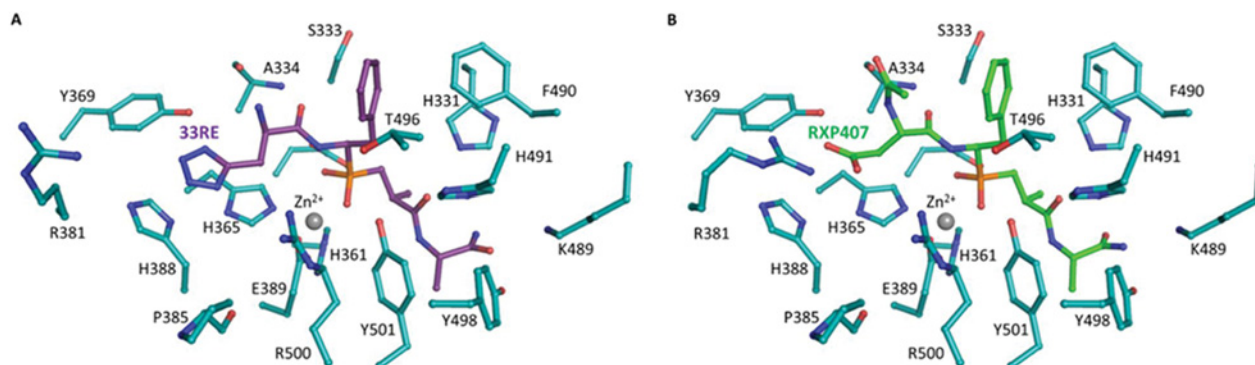


Figure 7 Comparison of the binding of compounds **33RE** and **RXP407** with N-domain ACE. Residues of N-domain ACE (cyan) interacting with (A) **33RE** (purple) and (B) **RXP407** (green; PDB code 3NXQ [34]) are shown as sticks.

design of novel N-selective ACE inhibitors could be a possible approach in combating tissue fibrosis diseases without affecting blood pressure.

Structure-based drug design is one major approach in developing novel drug candidates. SHOP methodology, an approach whereby information regarding the ligand is utilized to identify novel chemotypes with similar chemical attributes, has been utilized previously to develop novel inhibitor scaffolds of thrombin, human immunodeficiency virus protease and influenza neuraminidase [36]. This approach has also been used to develop new 5-lipoxygenase inhibitors [48]. More recently, this method has been modified into the form of receptor-based SHOP to make use of the information of the protein–ligand complex [37]. In this approach, geometrical descriptions of the active site and co-crystallized ligand are used to substitute a position of the ligand with other known fragments. The feasibility of the approach was confirmed with cyclin-dependent kinase 2 scaffolds using an enrichment study and further novel scaffolds and inhibitors have been designed for p38 mitogen-activated protein kinase [37]. This approach was employed using N-selective ligand **RXP407** to identify novel fragments that could be used in the design of N-selective ACE inhibitors.

Using the above receptor-based SHOP methodology, eight scaffolds were identified with known fragments that displayed equal or improved predicted interaction energies towards identified residues compared with **RXP407**. Specifically, the approach was able to identify fragments in the P₂ position that had predicted interaction energies with Tyr³⁶⁹ and Arg³⁸¹ similar to the **RXP407** P₂ aspartate residue. In the cases of Thr⁴⁹⁶ (S₁ subsite) and Thr³⁵⁸ (S₂' subsite), where **RXP407** has minimal contact with these unique N-domain residues, fragments were identified that had high predicted interaction energies. One such scaffold was synthesized using approaches that attempted to enhance the turnaround time of inhibitor production.

Assessment of inhibition was conducted using a fluorogenic (Abz)-FRK(Dnp)P assay. This analysis indicated that binding affinity of compound **33RE** to C- and N-domains, and therefore N-selectivity, is in the same range as that of the parent molecule. The data for **RXP407** presented here compare well with previously published reports [32,35]. Since both compounds had similar predicted interaction energies for the residues of interest,

it was anticipated that the N-selectivity of **33RE** would be comparable to **RXP407**. Kinetic analysis indicated three orders of magnitude N-selectivity for both compounds and serves as a proof of concept for using the discussed SHOP methodology in ACE inhibitor design. The co-crystal structure of N-domain ACE with **33RE** confirmed the interactions common to **RXP407** and highlighted the importance of the P₂ subsite for N-selectivity. The main difference in binding was seen in the loss of a salt bridge with Arg³⁸¹ but enhanced interactions with Tyr³⁶⁹. Importantly, these two residues are not conserved in the C-domain (replaced by Glu⁴⁰³ and Phe³⁹¹ respectively). Kinetic characterization revealed an 8-fold decrease in binding affinity for **33RE** upon mutating Arg³⁸¹ to Glu, suggesting an alternative orientation of this residue than that seen in the crystal structure. A 36-fold decrease in binding affinity was observed for Y369F confirming the structural findings of a loss of direct and water-mediated hydrogen bonds to the P₂ tetrazole of **33RE**. Thus, Tyr³⁶⁹ appears to be the major contributing residue towards the N-selectivity of compound **33RE**. The importance of the P₂ subsite for selectivity was further emphasized by the additive effect observed in YR/FE constituting a 250-fold decrease in **33RE**-binding affinity compared with wild-type, similar to that seen previously for **RXP407** [35]. Addition of the aromatic moiety also showed a stacking interaction with conserved residue His³⁸⁸, thus potentially improving affinity to both domains with a subsequent slight decrease in N-selectivity compared with parent molecule.

In conclusion, a modified SHOP methodology was employed to identify novel chemotypes with improved interactions with certain unique N-domain amino acid residues. A shortlist of scaffolds was identified and predicted to have equal or improved N-domain interactions compared with parent molecule **RXP407**. The most promising non-carboxylate P₂ candidate (compound **33RE**) was synthesized and displayed potent and N-selective inhibition. This novel phosphinic ACE inhibitor provides a basis for incorporation of non-amino acid and non-carboxylate P₂ functionalities into clinically relevant inhibitor backbones. It is noteworthy that a tetrazole moiety represents a bioisosteric replacement for a carboxylic acid group. N-domain selective inhibitors with drug-like characteristics could be useful in the treatment of tissue injury and fibrosis, which currently have limited treatment options.

CLINICAL PERSPECTIVES

- The N-domain catalytic site of ACE is highly selective for the antifibrotic and anti-inflammatory tetrapeptide *N*-acetyl-Ser-Asp-Lys-Pro. Thus a fragment-based approach was used to design a novel inhibitor that was specific for the N-domain.
- A molecule incorporating a tetrazole moiety in the P₂ position displayed potent inhibition of the N-domain and was 927-fold more selective for the N-domain than the C-domain. A crystal structure of the inhibitor in complex with the N-domain revealed its mode of binding through aromatic stacking with His³⁸⁸ and direct hydrogen bonding with the N-domain-specific Tyr³⁶⁹.
- This work further elucidates the molecular basis for N-domain-selective inhibition and assists in the design of novel N-selective ACE inhibitors that have potential for the treatment of fibrosis disorders

AUTHOR CONTRIBUTION

Geoffrey Masuyer and Ravi Acharya carried out the crystallography experiments, collected the data, analysed the data, and contributed to the writing of the paper; Edward Sturrock and Ross Douglas conceived and designed the study, and wrote the paper; Ismael Zamora carried out the fragment-based design of compound **33RE**; Lizelle Lubbe and Ross Douglas performed the kinetic experiments and analysed the data; and Kelly Chibale and Rajni Sharma designed and carried out the synthetic chemistry.

ACKNOWLEDGEMENTS

We gratefully acknowledge Ms Sylva Schwager for technical assistance. We also thank the scientists at PX station IO4-1, Diamond Light Source, Didcot, Oxon, U.K. for their support during X-ray diffraction data collection.

FUNDING

This work was supported by the University of Cape Town (U.C.T.) and the South African National Research Foundation (E.D.S., R.G.D. and L.L.). U.C.T., South African Medical Research Council and South African Research Chairs initiative of the Department of Science and Technology administered through the South African National Research Foundation are gratefully acknowledged for the support given to K.C. and R.K.S. The structural work was supported by the Medical Research Council (U.K.) through a project grant [grant number G1001685] and a Wellcome Trust (U.K.) equipment grant [grant number 088464 (to K.R.A.)].

REFERENCES

- Acharya, K. R., Sturrock, E. D., Riordan, J. F. and Ehlers, M. R. (2003) Ace revisited: a new target for structure-based drug design. *Nat. Rev. Drug Discovery* **2**, 891–902
- Fuhrquist, F. and Saijonna, O. (2008) Renin-angiotensin system revisited. *J. Intern. Med.* **264**, 224–236
- Soubrier, F., Alhenc-Gelas, F., Hubert, C., Allegrini, J., John, M., Tregear, G. and Corvol, P. (1988) Two putative active centers in human angiotensin I-converting enzyme revealed by molecular cloning. *Proc. Natl. Acad. Sci. U.S.A.* **85**, 9386–9390
- Wei, L., Alhenc-Gelas, F., Corvol, P. and Clauser, E. (1991) The two homologous domains of human angiotensin I-converting enzyme are both catalytically active. *J. Biol. Chem.* **266**, 9002–9008
- Natesh, R., Schwager, S. L., Sturrock, E. D. and Acharya, K. R. (2003) Crystal structure of the human angiotensin-converting enzyme–lisinopril complex. *Nature* **421**, 551–554
- Corradi, H. R., Schwager, S. L., Nchinda, A. T., Sturrock, E. D. and Acharya, K. R. (2006) Crystal structure of the N domain of human somatic angiotensin I-converting enzyme provides a structural basis for domain-specific inhibitor design. *J. Mol. Biol.* **357**, 964–974
- Jaspard, E., Wei, L. and Alhenc-Gelas, F. (1993) Differences in the properties and enzymatic specificities of the two active sites of angiotensin I-converting enzyme (kininase II). Studies with bradykinin and other natural peptides. *J. Biol. Chem.* **268**, 9496–9503
- Fuchs, S., Xiao, H. D., Cole, J. M., Adams, J. W., Frenzel, K., Michaud, A., Zhao, H., Keshelava, G., Capecchi, M. R., Corvol, P. and Bernstein, K. E. (2004) Role of the N-terminal catalytic domain of angiotensin-converting enzyme investigated by targeted inactivation in mice. *J. Biol. Chem.* **279**, 15946–15953
- Fuchs, S., Xiao, H. D., Hubert, C., Michaud, A., Campbell, D. J., Adams, J. W., Capecchi, M. R., Corvol, P. and Bernstein, K. E. (2008) Angiotensin-converting enzyme C-terminal catalytic domain is the main site of angiotensin I cleavage *in vivo*. *Hypertension* **51**, 267–274
- Rousseau, A., Michaud, A., Chauvet, M. T., Lenfant, M. and Corvol, P. (1995) The hemoregulatory peptide *N*-acetyl-Ser-Asp-Lys-Pro is a natural and specific substrate of the N-terminal active site of human angiotensin-converting enzyme. *J. Biol. Chem.* **270**, 3656–3661
- Lenfant, M., Wdziedzick-Bakala, J., Guittet, E., Prome, J. C., Sotty, D. and Frindel, E. (1989) Inhibitor of hematopoietic pluripotent stem cell proliferation: purification and determination of its structure. *Proc. Natl. Acad. Sci. U.S.A.* **86**, 779–782
- Lombard, M. N., Sotty, D., Wdziedzick-Bakala, J. and Lenfant, M. (1990) *In vivo* effect of the tetrapeptide, *N*-acetyl-Ser-Asp-Lys-Pro, on the G1-S transition of rat hepatocytes. *Cell Tissue Kinet.* **23**, 99–103
- Peng, H., Carretero, O. A., Brigstock, D. R., Oja-Tebbe, N. and Rhaleb, N. E. (2003) Ac-SDKP reverses cardiac fibrosis in rats with renovascular hypertension. *Hypertension* **42**, 1164–1170
- Yang, F., Yang, X. P., Liu, Y. H., Xu, J., Cingolani, O., Rhaleb, N. E. and Carretero, O. A. (2004) Ac-SDKP reverses inflammation and fibrosis in rats with heart failure after myocardial infarction. *Hypertension* **43**, 229–236
- Rasoul, S., Carretero, O. A., Peng, H., Cavin, M. A., Zhuo, J., Sanchez-Mendoza, A., Brigstock, D. R. and Rhaleb, N. E. (2004) Antifibrotic effect of Ac-SDKP and angiotensin-converting enzyme inhibition in hypertension. *J. Hypertens.* **22**, 593–603
- Peng, H., Carretero, O. A., Vuljaj, N., Liao, T. D., Motivala, A., Peterson, E. L. and Rhaleb, N. E. (2005) Angiotensin-converting enzyme inhibitors: a new mechanism of action. *Circulation* **112**, 2436–2445
- Peng, H., Carretero, O. A., Liao, T. D., Peterson, E. L. and Rhaleb, N. E. (2007) Role of *N*-acetyl-seryl-aspartyl-lysyl-proline in the antifibrotic and anti-inflammatory effects of the angiotensin-converting enzyme inhibitor captopril in hypertension. *Hypertension* **49**, 695–703
- Lin, C. X., Rhaleb, N. E., Yang, X. P., Liao, T. D., D'Ambrosio, M. A. and Carretero, O. A. (2008) Prevention of aortic fibrosis by *N*-acetyl-seryl-aspartyl-lysyl-proline in angiotensin II-induced hypertension. *Am. J. Physiol. Heart Circ. Physiol.* **295**, H1253–H1261
- Liao, T. D., Yang, X. P., D'Ambrosio, M., Zhang, Y., Rhaleb, N. E. and Carretero, O. A. (2010) *N*-acetyl-seryl-aspartyl-lysyl-proline attenuates renal injury and dysfunction in hypertensive rats with reduced renal mass: council for high blood pressure research. *Hypertension* **55**, 459–467

- 20 Wang, M., Liu, R., Jia, X., Mu, S. and Xie, R. (2010) N-acetyl-seryl-aspartyl-lysyl-proline attenuates renal inflammation and tubulointerstitial fibrosis in rats. *Int. J. Mol. Med.* **26**, 795–801
- 21 Rhaleb, N. E., Pokharel, S., Sharma, U. and Carretero, O. A. (2011) Renal protective effects of N-acetyl-Ser-Asp-Lys-Pro in deoxycorticosterone acetate-salt hypertensive mice. *J. Hypertens.* **29**, 330–338
- 22 Sun, Y., Yang, F., Yan, J., Li, Q., Wei, Z., Feng, H., Wang, R., Zhang, L. and Zhang, X. (2010) New anti-fibrotic mechanisms of n-acetyl-seryl-aspartyl-lysyl-proline in silicon dioxide-induced silicosis. *Life Sci.* **87**, 232–239
- 23 Xu, H., Yang, F., Sun, Y., Yuan, Y., Cheng, H., Wei, Z., Li, S., Cheng, T., Brann, D. and Wang, R. (2012) A new antifibrotic target of Ac-SDKP: inhibition of myofibroblast differentiation in rat lung with silicosis. *PLoS ONE* **7**, e40301
- 24 Zhang, L., Xu, L. M., Chen, Y. W., Ni, Q. W., Zhou, M., Qu, C. Y. and Zhang, Y. (2012) Antifibrotic effect of N-acetyl-seryl-aspartyl-lysyl-proline on bile duct ligation induced liver fibrosis in rats. *World J. Gastroenterol.* **18**, 5283–5288
- 25 Li, P., Xiao, H. D., Xu, J., Ong, F. S., Kwon, M., Roman, J., Gal, A., Bernstein, K. E. and Fuchs, S. (2010) Angiotensin-converting enzyme N-terminal inactivation alleviates bleomycin-induced lung injury. *Am. J. Pathol.* **177**, 1113–1121
- 26 Azizi, M., Rousseau, A., Ezan, E., Guyene, T. T., Michelet, S., Grognet, J. M., Lenfant, M., Corvol, P. and Menard, J. (1996) Acute angiotensin-converting enzyme inhibition increases the plasma level of the natural stem cell regulator N-acetyl-seryl-aspartyl-lysyl-proline. *J. Clin. Invest.* **97**, 839–844
- 27 Redelinghuys, P., Nchinda, A. T. and Sturrock, E. D. (2005) Development of domain-selective Angiotensin I-converting enzyme inhibitors. *Ann. N.Y. Acad. Sci.* **1056**, 160–175
- 28 Wei, L., Clauser, E., Alhenc-Gelas, F. and Corvol, P. (1992) The two homologous domains of human angiotensin I-converting enzyme interact differently with competitive inhibitors. *J. Biol. Chem.* **267**, 13398–13405
- 29 Nussberger, J., Cugno, M., Amstutz, C., Cicardi, M., Pellacani, A. and Agostoni, A. (1998) Plasma bradykinin in angio-oedema. *Lancet* **351**, 1693–1697
- 30 Emanuelli, C., Grady, E. F., Madeddu, P., Figini, M., Bunnett, N. W., Parisi, D., Regoli, D. and Geppetti, P. (1998) Acute ACE inhibition causes plasma extravasation in mice that is mediated by bradykinin and substance P. *Hypertension* **31**, 1299–1304
- 31 Adam, A., Cugno, M., Molinaro, G., Perez, M., Lepage, Y. and Agostoni, A. (2002) Aminopeptidase P in individuals with a history of angioedema on ACE inhibitors. *Lancet* **359**, 2088–2089
- 32 Dive, V., Cotton, J., Yiotakis, A., Michaud, A., Vassiliou, S., Jiracek, J., Vazeux, G., Chauvet, M. T., Cuniassse, P. and Corvol, P. (1999) RXP 407, a phosphinic peptide, is a potent inhibitor of angiotensin I converting enzyme able to differentiate between its two active sites. *Proc. Natl. Acad. Sci. U.S.A.* **96**, 4330–4335
- 33 Sharma, R. K., Douglas, R. G., Louw, S., Chibale, K. and Sturrock, E. D. (2012) New ketomethylene inhibitor analogues: synthesis and assessment of structural determinants for N-domain selective inhibition of angiotensin-converting enzyme. *Biol. Chem.* **393**, 485–493
- 34 Anthony, C. S., Corradi, H. R., Schwager, S. L., Redelinghuys, P., Georgiadis, D., Dive, V., Acharya, K. R. and Sturrock, E. D. (2010) The N domain of human angiotensin-I-converting enzyme: the role of N-glycosylation and the crystal structure in complex with an N domain-specific phosphinic inhibitor, RXP407. *J. Biol. Chem.* **285**, 35685–35693
- 35 Kroger, W. L., Douglas, R. G., O'Neill, H. G., Dive, V. and Sturrock, E. D. (2009) Investigating the domain specificity of phosphinic inhibitors RXP4380 and RXP407 in angiotensin-converting enzyme. *Biochemistry* **48**, 8405–8412
- 36 Bergmann, R., Linusson, A. and Zamora, I. (2007) SHOP: scaffold HOPping by GRID-based similarity searches. *J. Med. Chem.* **50**, 2708–2717
- 37 Bergmann, R., Liljefors, T., Sorensen, M. D. and Zamora, I. (2009) SHOP: receptor-based scaffold HOPping by GRID-based similarity searches. *J. Chem. Inf. Model* **49**, 658–669
- 38 Dixon, M. (1953) The determination of enzyme inhibitor constants. *Biochem. J.* **55**, 170–171
- 39 Ehlers, M. R., Chen, Y. N. and Riordan, J. F. (1991) Purification and characterization of recombinant human testis angiotensin-converting enzyme expressed in Chinese hamster ovary cells. *Protein Expr. Purif.* **2**, 1–9
- 40 Kabsch, W. (2010) XDS. *Acta Crystallogr., Sect. D: Biol. Crystallogr.* **66**, 125–132
- 41 Collaborative Computational Project Number 4 (1994) The CCP4 suite: programs for protein crystallography. *Acta Crystallogr., Sect. D: Biol. Crystallogr.* **50**, 760–763
- 42 McCoy, A. J., Grosse-Kunstleve, R. W., Adams, P. D., Winn, M. D., Storoni, L. C. and Read, R. J. (2007) Phaser crystallographic software. *J. Appl. Crystallogr.* **40**, 658–674
- 43 Murshudov, G. N., Vagin, A. A. and Dodson, E. J. (1997) Refinement of macromolecular structures by the maximum-likelihood method. *Acta Crystallogr., Sect. D: Biol. Crystallogr.* **53**, 240–255
- 44 Emsley, P. and Cowtan, K. (2004) Coot: model-building tools for molecular graphics. *Acta Crystallogr., Sect. D: Biol. Crystallogr.* **60**, 2126–2132
- 45 Schuttelkopf, A. W. and van Aalten, D. M. (2004) PRODRG: a tool for high-throughput crystallography of protein-ligand complexes. *Acta Crystallogr. D* **60**, 1355–1363
- 46 Davis, I. W., Leaver-Fay, A., Chen, V. B., Block, J. N., Kapral, G. J., Wang, X., Murray, L. W., Arendall, III, W. B., Snoeyink, J., Richardson, J. S. and Richardson, D. C. (2007) MolProbity: all-atom contacts and structure validation for proteins and nucleic acids. *Nucleic Acids Res.* **35**, W375–W383
- 47 McDonald, I. K. and Thornton, J. M. (1994) Satisfying hydrogen bonding potential in proteins. *J. Mol. Biol.* **238**, 777–793
- 48 Aparoy, P., Reddy, K. K. and Reddanna, P. (2012) Structure and ligand based drug design strategies in the development of novel 5-LOX inhibitors. *Curr. Med. Chem.* **19**, 3763–3778
- 49 Wallace, A. C., Laskowski, R. A. and Thornton, J. M. (1996) LIGPLOT: a program to generate schematic diagrams of protein-ligand interactions. *Protein Eng.* **8**, 8
- 50 Georgiadis, D., Beau, F., Czarny, B., Cotton, J., Yiotakis, A. and Dive, V. (2003) Roles of the two active sites of somatic angiotensin-converting enzyme in the cleavage of angiotensin I and bradykinin: insights from selective inhibitors. *Circ. Res.* **93**, 148–154
- 51 Nchinda, A. T., Chibale, K., Redelinghuys, P. and Sturrock, E. D. (2006) Synthesis and molecular modeling of a lisinopril-tryptophan analogue inhibitor of angiotensin I-converting enzyme. *Bioorg. Med. Chem. Lett.* **16**, 4616–4619
- 52 Nchinda, A. T., Chibale, K., Redelinghuys, P. and Sturrock, E. D. (2006) Synthesis of novel keto-ACE analogues as domain-selective angiotensin I-converting enzyme inhibitors. *Bioorg. Med. Chem. Lett.* **16**, 4612–4615

Received 19 July 2013/20 August 2013; accepted 9 September 2013

Published as Immediate Publication 9 September 2013, doi: 10.1042/CS20130403

SUPPLEMENTARY ONLINE DATA

Fragment-based design for the development of N-domain-selective angiotensin-1-converting enzyme inhibitors

Ross G. DOUGLAS*¹, Rajni K. SHARMA†¹, Geoffrey MASUYER‡, Lizelle LUBBE*, Ismael ZAMORA§, K. Ravi ACHARYA‡, Kelly CHIBALE† and Edward D. STURROCK*

*Institute of Infectious Disease and Molecular Medicine, and Division of Medical Biochemistry, University of Cape Town, Observatory, Cape Town 7935, South Africa

†Department of Chemistry and Institute of Infectious Disease and Molecular Medicine, University of Cape Town, Rondebosch, Cape Town 7701, South Africa

‡Department of Biology and Biochemistry, University of Bath, Claverton Down, Bath BA2 7AY, U.K.

§Lead Molecular Design, Sant Cugat del Vallès and Pompeu Fabra University, Barcelona, Spain

MATERIALS AND METHODS

SHOP search

The methodology to perform a SHOP search consists of several steps [1]. (i) A database of fragments with the potential to replace P₂–P₂' groups was built. The database was prepared using commercially available building blocks: Aldrich, Bionet, CombiBlocks Enamine, Maybridge, Specs and Synthonix. The commercial structures were submitted to a virtual reaction algorithm, where each of the hypothetical interactions of the compounds is replaced by an anchor point, following the reaction pattern. The virtual compounds built in this way were converted into 3D and a conformational analysis performed using the algorithm implemented in SHOP. For each final structure a set of descriptors were computed: Shop-Geom, Shop-GRID, Shop-Shape and Shop-Finger. (ii) The database is screened using the ligand–receptor complex (PDB code 3NXQ; N-domain crystallized with inhibitor RXP407) [2]. The fragment shown in Figure S1 was the one used to define the region in the protein where the computation was carried out. (iii) A descriptor-based similarity analysis was performed comparing the query and the fragments in the database, and generating a list of ranked fragments that may replace the query. In this procedure, once the fragment has been selected in the ligand, it was removed from the ligand–receptor complex and a GRID computation in the protein cavity performed (Figure S2). There are four parameters that can be modified during this process: protein filtering (PF) option: the 'none' level was chosen in this computation which means that no atom is deleted from the protein; the grid clearance was set to 2 Å in all searches done; the cut-off parameter was set to 1.5 Å; and ligand filtering (LF) was set to one.

In Figure S2 the interaction fields in the regions of interest are shown. Four amino acids differing in chemical nature from

their C-domain counterparts were selected. Residues Tyr³⁶⁹ and Arg³⁸¹ are located in the S₂ subsite and have been shown by both mutagenesis and structural studies to be important for selective RXP407 binding [2,3]. These amino acids are replaced by Phe³⁹¹ and Glu⁴⁰³, respectively, in the C-domain (all C-domain residues are given as tACE numbering). Thr⁴⁹⁶ is located on the border of the S₂ and S₁ subsites [4]. Owing to its proximity to the RXP407 phenylalanine residue and the lack of hydrogen bonding potential of the corresponding C-domain residue (Val⁵¹⁸), it was selected as a side chain for further selective binding exploitation by hydrogen bonding. Thr³⁵⁸ is located in the S₂' subsite and differs from the corresponding C-domain residue Val³⁸⁰ [3]. As with Thr⁴⁹⁶, identification of functional groups that allow for specific interaction with the Thr side chain by hydrogen bonding could assist in generating N-selective inhibitors. (iv) The selected fragments were then aligned with the query and placed in the protein cavity. If there were no collisions with the protein atoms (within a certain tolerance), the fragment was selected for further analysis. (v) Finally, the newly built molecule was optimized in the protein cavity and the calculation of the energy of interaction between the new ligand and the amino acids in the protein was performed by translating every atom from the ligand into a GRID atom type and calculating the interaction using the POSI directive in GRID.

At the end of the modelling process, the poses were confirmed visually. Top ranking molecules that had reasonable poses (compared with previous structures) were selected for further study.

Synthesis

(*R/S*)-2-methyl-3-(((*R*)-1-(*N*-(benzyloxycarbonyl)amino)-2-phenylethyl)-hydroxyphosphinyl)propanoic acid, ethylester (**1**)
The commercially available (*R*)-((1-(*N*-benzyloxycarbonyl)

¹These authors contributed equally to this work.

Correspondence: Professor Edward D. Sturrock (email edward.sturrock@uct.ac.za), Professor Kelly Chibale (email kelly.chibale@uct.ac.za) or Professor K. Ravi Acharya (email K.R.Acharya@bath.ac.uk).

amino)-2-phenylethyl)phosphinic acid (571 mg, 1.78 mmol, 1 equiv.) and hexamethyldisilazane (2.1 ml, 8.9 mmol, 5 equiv.) were heated at 110 °C for 2 h under argon, then cooled to 60 °C. At this temperature ethyl methacrylate (0.335 ml, 2.67 mmol, 1.5 equiv.) was added dropwise and the resulting solution was stirred for 3 h at 90 °C. The reaction mixture was cooled to 60 °C, methanol (5 ml) was added dropwise, and stirred at 25 °C for 20 min. The mixture was concentrated and the residue was dissolved in a mixture of 5% aqueous NaHCO₃ (10 ml) and diethyl ether (15 ml). The organic phase was separated and the aqueous phase washed twice with ether (10 ml × 2). The aqueous phase was acidified with 5% aqueous HCl to pH 1–2, the compound extracted with ethyl acetate (15 ml × 3), and combined organic phase dried with MgSO₄ and concentrated under vacuum to produce a white solid. Purification by silica gel chromatography using dichloromethane/methanol (8:2) as eluent, afforded diastereomeric mixture (4:2) of (*R/S*)-2-methyl-3-(((*R*)-1-(*N*-(benzyloxycarbonyl)amino)-2-phenylethyl)-hydroxyphosphinyl)propanoic acid, ethylester **1** (520 mg) as white solid with 67% yield. ¹H NMR(300 MHz, CDCl₃): δ 7.30–7.16(10H, m, Ar-H), 5.33(1H, d, 9.1 Hz, -NH), 4.97(2H, s, -OCH₂Ph), 4.27–4.02(3H, m, *CHPCH*₂, OCH₂CH₃), 3.30–3.24(1H, m, PCHCHHPh), 2.92–2.80(2H, m, PCHCHHPh, PCH₂CH), 2.28–2.19(1H, m, PCHHCH), 1.83–1.74(1H, m, -PCHHCH), 1.25 (3H, d, *J* 6.9 Hz, *CHPCH*₂CH(CH₃)), 1.21(3H, d, *J* 7 Hz, OCH₂CH₃); ¹³C NMR(100 MHz, CDCl₃): δ 175.5, 156.1, 136.7, 136.3, 129.1(2C), 128.5(2C), 128.4, 128.2(2C), 127.8(2C), 126.7, 66.9, 61, 52.2, 33.8, 30.8, 29.9, 18.9, 14.1; ³¹P NMR (162 MHz, CDCl₃): δ 52.3, 50.5; LC-ESI-MS(+ve): *m/z* 434.2[M + H]⁺.

(*R/S*)-2-methyl-3-(((*R*)-1-(*N*-(benzyloxycarbonyl)amino)-2-phenylethyl)-adamantylphosphinyl)propanoic acid, ethylester (**2**).

To a refluxing solution of phosphinate **1** (600 mg, 1.38 mmol, 1 equiv.) and 1-adamantyl bromide (357 mg, 1.65 mmol, 1.2 equiv.) in chloroform (20 ml) silver (I) oxide (383 mg, 1.65 mmol, 1.2 equiv.) was added portionwise over 50 min. This solution was refluxed for an additional 2 h and then concentrated. The residue was treated with diethyl ether (20 ml), filtered through celite and concentrated. The residue was purified by silica gel chromatography using dichloromethane/isopropanol (95:5) as eluent and yielded a mixture of (*R/S*)-2-methyl-3-(((*R*)-1-(*N*-(benzyloxycarbonyl)amino)-2-phenylethyl)-adamantylphosphinyl)propanoic acid, ethylester **2** (657 mg, 84%) as a colourless liquid.

¹H NMR(300 MHz, CDCl₃): δ 7.29–7.20(10H, m, Ar-H), 4.96(2H, s, -OCH₂Ph), 4.17–4.09(3H, m, *CHPCH*₂, OCH₂CH₃), 3.29–3.23(1H, m, PCHCHHPh), 2.89–2.80(2H, m, PCHCHHPh, PCH₂CH), 2.38–2.29(1H, m, PCHHCH), 2.17–2.06(9H, m, *CH* of Ad group, *CCH*₂ of Ad group), 1.74–1.62(7H, m, PCHH, *CCH*₂CH of Ad group), 1.25 (3H, d 6.9 Hz, *CHPCH*₂CH(CH₃)), 1.21(3H, d, *J* 6.9 Hz, OCH₂CH₃); ¹³C NMR (100 MHz, CDCl₃): δ 166.9, 155.9, 137, 136.4, 129.3, 129.2(2C), 128.4, 128(2C), 127.9(2C), 127.8, 126.6, 81.7, 66.9, 60.8, 52.7, 44.5(3C), 35.7(3C), 34.1, 31.2(3C), 30.8, 30.7, 19.2, 14.1; ³¹P NMR (162 MHz, CDCl₃): δ 47.5, 46.3; LC-ESI-MS(+ve): *m/z* 568.2[M + H]⁺.

(*R/S*)-2-methyl-3-(((*R*)-1-(*N*-(benzyloxycarbonyl)amino)-2-phenylethyl)-adamantylphosphinyl)propanoic acid (**3**).

The solution of pseudo dipeptide **2** (100 mg, 0.176 mmol) in methanol (5 ml) was treated with 4 M aqueous NaOH solution (0.4 ml) and the reaction mixture was stirred for 2 h at room temperature. The solvent was removed and the residue was diluted with H₂O (10 ml) and acidified with 5% aqueous HCl in an ice-water bath to pH 2. The aqueous phase was extracted with EtOAc ethyl acetate (20 ml × 2) and the combined organic layer was dried with MgSO₄ and concentrated to yield a mixture of (*R/S*)-2-methyl-3-(((*R*)-1-(*N*-(benzyloxycarbonyl)amino)-2-phenylethyl)-adamantylphosphinyl)propanoic acid **3** (70 mg, 74%) as a white solid.

¹H NMR(300 MHz, CDCl₃): δ 7.30–7.14(10H, m, Ar-H), 4.90(2H, s, -OCH₂Ph), 4.24–4.20(1H, m, *CHPCH*₂), 3.18–3.13(1H, m, PCHCHHPh), 2.83–2.76(2H, m, PCHCHHPh, PCH₂CH), 2.37–2.25(1H, m, PCHHCH), 2.11–1.97 (9H, m, *CH* of Ad group, *CCH*₂ of Ad group), 1.74–1.62(7H, m, PCHH, *CCH*₂CH of Ad group), 1.19(3H, d *J* 7.1 Hz, *CHPCH*₂CH(CH₃)); ¹³C NMR(100 MHz, DMSO): δ 177, 156.3, 138.6, 137.6, 129.3, 128.4(4C), 128(2C), 127.6(2C), 126.6, 81.7, 65.6, 54.7, 44.3(3C), 35.8(3C), 33.8, 31(3C), 30.5, 29.6, 19.6; ³¹P NMR(162 MHz, DMSO): 47.5, 47.5; LC-ESI-MS(+ve): *m/z* 540.2[M + H]⁺.

[(*R/S*)-2-methyl-3-(((*R*)-1-(*N*-(benzyloxycarbonyl)amino)-2-phenylethyl)-adamantylphosphinyl)propanoyl]amino]-(*S*)-2-propanamide (**4**).

To a solution of pseudo phosphinic acid **3** (480 mg, 0.892 mmol, 1 equiv.) in dichloromethane (5 ml), EDC.HCl (188 mg, 0.981 mmol, 1.1 equiv.), L-alaninamide. HCl (122 mg, 0.981 mmol, 1.1 equiv.), HOBt (129 mg, 0.981 mmol, 1.1 equiv.), DIPEA (0.311 ml, 1.78 mmol, 2 equiv.) were added at 0 °C, and the mixture was stirred for 18 h at room temperature. H₂O was added and the aqueous phase was extracted with ethyl acetate (30 ml × 3). The combined organic layer was washed with H₂O (10 ml), brine (10 ml), dried over MgSO₄ and concentrated. The residue was purified over silica gel chromatography using 5% dichloromethane/methanol as eluent and afforded [(*R/S*)-2-methyl-3-(((*R*)-1-(*N*-(benzyloxycarbonyl)amino)-2-phenylethyl)-adamantylphosphinyl)propanoyl]amino]-(*S*)-2-propanamide **4** (0.543 g, 73%) as a yellow liquid.

¹H NMR(300 MHz, CDCl₃): δ 7.27–7.16 (12H, m, Ar-H, CONH₂), 4.97(2H, s, -OCH₂Ph), 4.49–4.30(1H, m, *CHCONH*₂), 4.21–4.16(1H, m, *CHPCH*₂), 3.22–3.11(1H, m, PCHCHHPh), 2.79–2.67(2H, m, PCHCHHPh, PCH₂CH), 2.31–2.22(1H, m, PCHHCH), 2.14–2.07 (9H, m, *CH* of Ad group, *CCH*₂ of Ad group), 1.78–1.56(7H, m, PCHH, *CCH*₂CH of Ad group), 1.35(3H, d, 7.2 Hz, CH(CH₃)CONH₂), 1.10(3H, d, *J* 6.4 Hz, *CHPCH*₂CH(CH₃)); ¹³C NMR (100 MHz, CDCl₃): δ 175.8, 174.7, 156.6, 136.9, 136.8, 129.2, 129.1(2C), 128.5(2C), 128.1(2C), 127.9, 127.8, 126.7, 83.5, 67.1, 52.9, 49, 44.6(3C), 35.6(3C), 34.2, 31.2(3C), 30.7, 29.6, 17.7, 17.1; ³¹P NMR(162 MHz, CDCl₃): 47.1, 46.1; LC-ESI-MS(+ve): *m/z* 610.7[M + H]⁺.

[(*R/S*)-2-methyl-3-(((*R*)-1-(amino)-2-phenylethyl)-adamantylphosphinyl)propanoyl] amino]-(*S*)-2-propanamide (**5**).

To a solution of **4** (140 mg, 0.229 mmol) in MeOH (30 ml) 10% Pd/C (50 mg) was added and stirred in under 4 psi

(1 psi = 6.9 kPa) of hydrogen for 4-6 h. The reaction mixture was filtered using celite, washed with EtOH (50 ml), and evaporation of solvent under vacuum afforded [(*R/S*)-2-methyl-3-(((*R*)-1-(amino)-2-phenylethyl)-adamantylphosphinyl)propanoyl] amino]-(*S*)-2-propanamide **5** (82 mg, 75%) as a yellow liquid.

¹H NMR(300 MHz, CDCl₃): δ 7.27-7.16(7H, m, Ar-H, CONH₂), 5.44(2H, m, CHNH₂), 4.49-4.30(1H, m, CHCONH₂), 4.21-4.16(1H, m, CHPCH₂), 3.22-3.11(1H, m, PCHCHHPh), 2.79-2.67(2H, m, PCHCHHPh, PCH₂CH), 2.31-2.22(1H, m, PCHHCH), 2.14-2.07 (9H, m, CH of Ad group, CCH₂ of Ad group), 1.78-1.56(7H, m, PCHH, CCH₂CH of Ad group), 1.35(3H, d, 7.2 Hz, CH(CH₃)CONH₂), 1.10(3H, d, 6.4 Hz, CHPCH₂CH(CH₃)); LC-ESI-MS(+ve): *m/z* 476.3[M+H]⁺.

[(*S*)-((3-1H-tetrazol-2-yl)-2-aminopropanoyl)-[(*S*)-2-methyl-3-(((*R*)-1-(amino)-2-phenylethyl)-adamantylphosphinyl)propanoyl]amino]-(*S*)-2-propanamide (**33RE**).

To a solution of **5** (90 mg, 0.188 mmol, 1 equiv.) in dichloromethane (5 ml), EDC.HCl (39 mg, 0.207 mmol, 1.1 equiv.), 3-tetrazolyl-2-(1,1-dimethylethoxy)-methanamide propionic acid (53 mg, 0.207 mmol, 1.1 equiv.), HOBt (28 mg,

0.207 mmol, 1.1 equiv.), DIPEA (0.066 ml, 0.376 mmol, 2 equiv.) were added at 0°C. H₂O was added and the aqueous phase was extracted with ethyl acetate (30 ml×3). The combined organic layer was washed with H₂O (10 ml), brine (10 ml), dried over MgSO₄ and concentrated. The residue was treated with a mixture of TFA/DCM/anisole/H₂O (4.5/0.4/0.1/0.1) for 3 h at room temperature. Evaporation of the solvent afforded the crude product which was chromatographed using reverse-phase HPLC to yield two diastereoisomers. The active component (**33RE**) of the above diastereoisomeric mixture, corresponds to the first fraction that eluted and to 10% of the total amount of tripeptide (*t_R* = 6.04).

¹H NMR(300 MHz, CD₃OD): δ 7.29-7.17(7H, m, Ar-H, CONH₂), 4.86(2H, m, CHNH₂), 4.51(1H, dd, 3.2 11.7 Hz, NH₂CH Tetrazole), 4.21(1H, t, *J* 4.7 Hz, CHPCH₂), 4.09(1H, q, *J* 7.2 Hz, CHCONH₂), 3.70(1H, dd, 5 15.9 Hz, NH₂CHCHH Tetrazole), 3.59(1H, dd, *J* 4.7 15.9 Hz, NH₂CHCHH Tetrazole), 2.91-2.75(3H, m, PCHCH₂Ph, PCH₂CH), 2.28-2.17(1H, m, PCHHCH), 1.77-1.66(1H, m, PCHH), 1.31(3H, d, *J* 7.7 Hz, CH(CH₃)CONH₂), 1.29(3H, d, *J* 7.3 Hz, CHPCH₂CH(CH₃)); LC-ESI-MS(+ve): *m/z* 481.6[M+H]⁺.

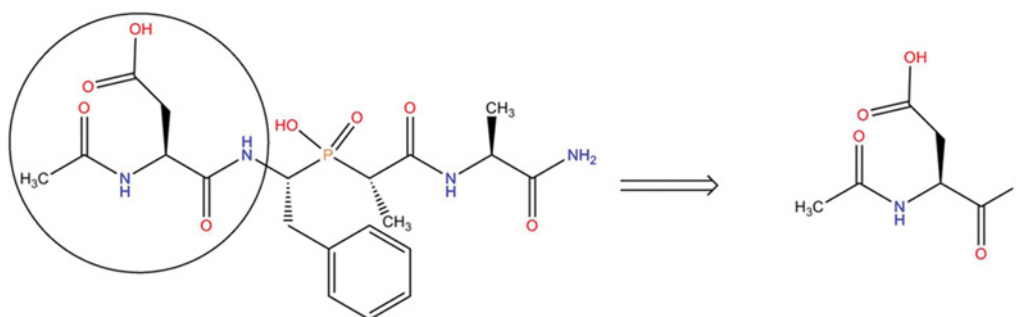
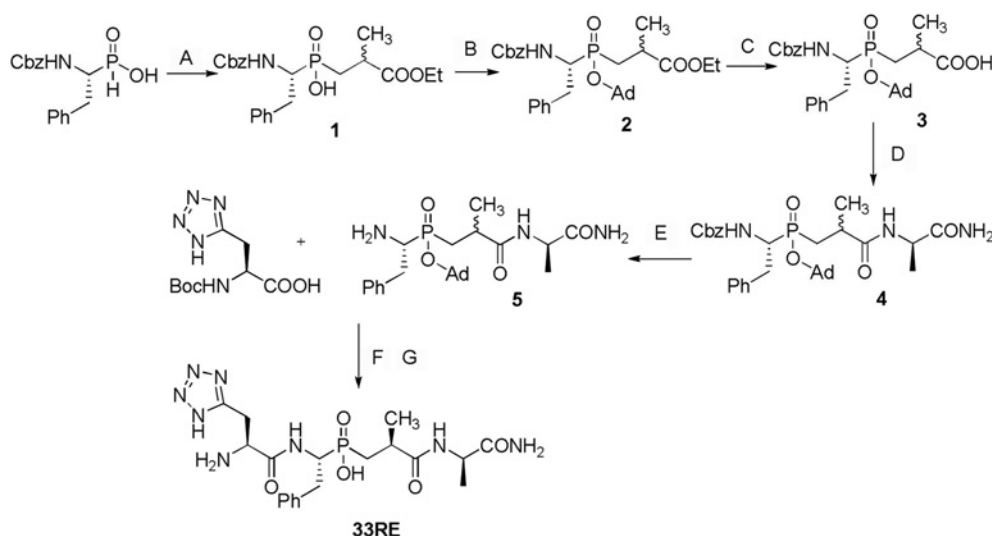


Figure S1 Query fragment that was used to define the region where the computation is performed



Scheme S1 Synthetic protocol for compound **33RE**

Reactant and reagents: (A) ethyl methacrylate, HMDS, DIPEA, 110°C, 5 h; (B) 1-adamantyl bromide, Ag₂O, CHCl₃, 5 h; (C) NaOH, MeOH, 2 h; (D) L-alaninamide, EDC.HCl, HOBt, DIPEA, DCM, 18 h; (E) 10% Pd/C, H₂, 8 h; (F) EDC.HCl, HOBt, DIPEA, DCM, 18 h; (G) TFA/anisole/H₂O/DCM, 3 h.

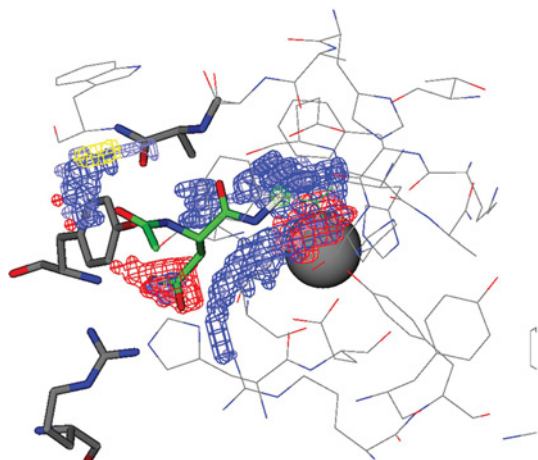


Figure S2 GRID molecular interaction fields that are computed in the region where the fragment is selected

The blue field is obtained by the N1 probe and represents H-bond donor regions, the red field is obtained using the O probe and represents H-Bond acceptor regions and the yellow field is obtained using the DRY probe and represents hydrophobic regions.

REFERENCES

- 1 Bergmann, R., Liljefors, T., Sorensen, M. D. and Zamora, I. (2009) SHOP: receptor-based scaffold HOPping by GRID-based similarity searches. *J. Chem. Inf. Model* **49**, 658–669
- 2 Anthony, C. S., Corradi, H. R., Schwager, S. L., Redelinghuys, P., Georgiadis, D., Dive, V., Acharya, K. R. and Sturrock, E. D. (2010) The N domain of human angiotensin-I-converting enzyme: the role of N-glycosylation and the crystal structure in complex with an N domain-specific phosphinic inhibitor, RXP407. *J. Biol. Chem.* **285**, 35685–35693
- 3 Kroger, W. L., Douglas, R. G., O'Neill, H. G., Dive, V. and Sturrock, E. D. (2009) Investigating the domain specificity of phosphinic inhibitors RXPA380 and RXP407 in angiotensin-converting enzyme. *Biochemistry* **48**, 8405–8412
- 4 Wei, L., Alhenc-Gelas, F., Corvol, P and Clauser, E. (1991) The two homologous domains of human angiotensin I-converting enzyme are both catalytically active. *J. Biol. Chem.* **266**, 9002–9008

Received 19 July 2013/20 August 2013; accepted 9 September 2013

Published as Immediate Publication 9 September 2013, doi: 10.1042/CS20130403